Supporting Information

Deterministic mode analysis for InP plasmonic nanowire lasers

*Yu-Shi Tsai, Hung-Jung Shen, Chia-Hung Wu, Guan-Ting Lin, Kuo-Ping Chen, Jhih-Sheng Wu, and Tien-Chang Lu**

Y.-S. Tsai, J.-S Wu, and T.-C. Lu
Department of Photonics, College of Electrical and Computer Engineering
National Yang Ming Chiao Tung University
Hsinchu 30010, Taiwan

H.-J. Shen, G.-T. Lin, and K.-P. Chen
Institute of Photonics Technologies, College of Electrical and Computer Engineering
National Tsing Hua University
Hsinchu 30013, Taiwan

C.-H. Wu
College of Photonics
National Yang Ming Chiao Tung University
Hsinchu 30010, Taiwan

*E-mail: timtclu@nycu.edu.tw

Keywords: nanolasers, surface plasmon polaritons, InP nanowire, graphene, mode analysis

Outline

- The transfer printing process for InP nanowire
- Raman spectrum on graphene / single-crystalline Au flake
- Dispersion of the effective refractive index for InP nanowires with varying diameters
- Determination of the dominant mode in InP nanowires on SiO_2 and single-crystalline Au flake
- Band diagram of Au and monolayer graphene
- References

■ The transfer printing process for InP nanowire

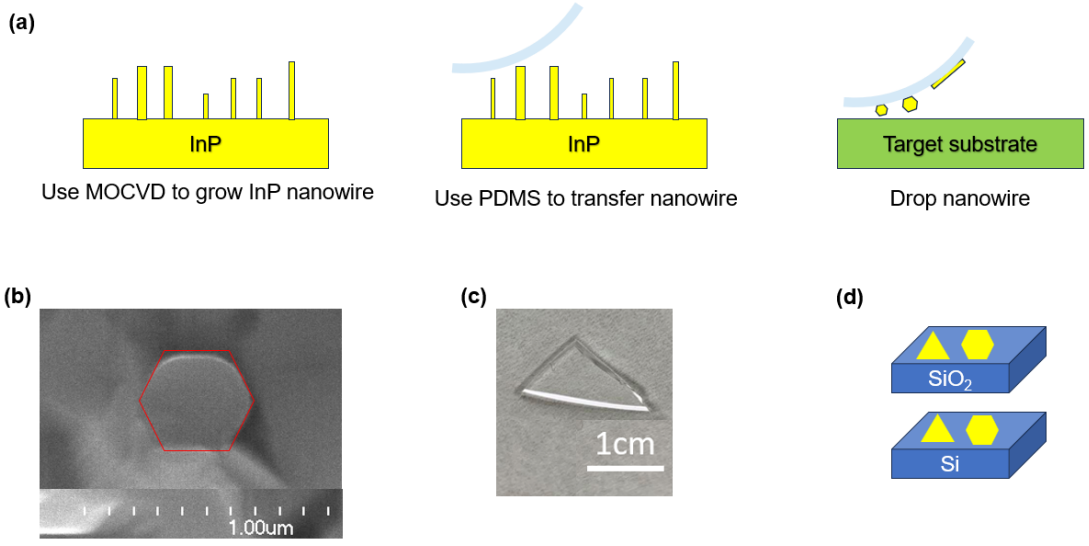

Figure S1 | Steps of the transfer printing process and images of the InP nanowire. **(a)** Transfer steps of InP nanowires to the target substrate. **(b)** SEM image showing the nanowire facet. **(c)** OM image of a PDMS stamp used for transfer. **(d)** Schematic of the target substrate with metal flakes.

The InP nanowires used in this study were synthesized by metal-organic chemical-vapor deposition (MOCVD), as detailed in the Experimental Section of the main text. Due to their wurtzite crystal structure, the nanowire facets exhibit a characteristic hexagonal shape [1], which is evident from the SEM image in **Fig. S1(b)**. The nanowires were subsequently transferred to target substrates using a Polydimethylsiloxane (PDMS) stamp, as shown in **Fig. S1(c)**. Two types of substrates were employed, illustrated in **Fig. S1(d)**. Because the refractive index of silicon is close to that of InP, strong optical leakage into the substrate occurs, rendering silicon unsuitable for supporting photonic modes. To mitigate this issue, SiO_2 substrates were used for photonic mode investigations.

■ Raman spectrum on graphene/ single-crystalline Au flake

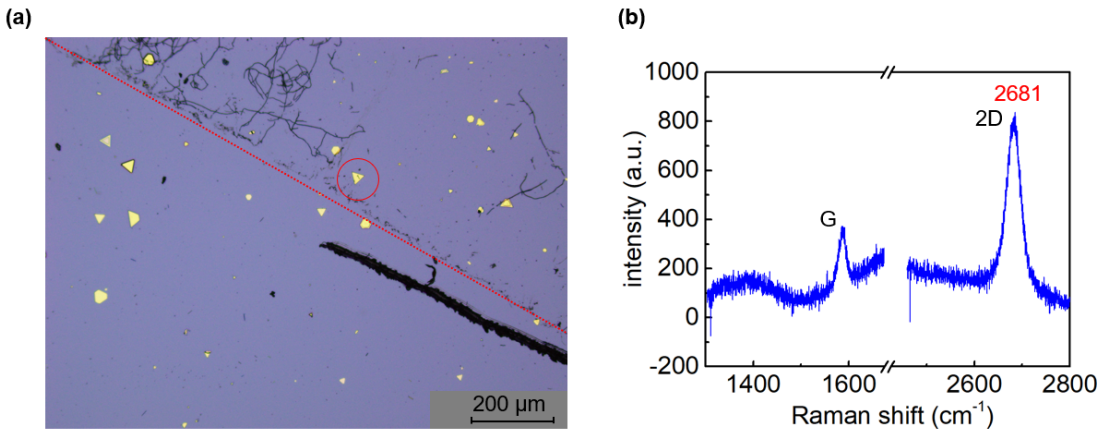

Figure S2 | Substrate covered with graphene and corresponding Raman spectrum. **(a)** OM image of substrate covered with a monolayer graphene. The yellow triangular and polygonal flakes are Au. **(b)** Raman spectrum of graphene measured on the single-crystalline Au flake within the red-circled region shown in (a).

After transferring the monolayer graphene onto the substrate, the optical microscopy (OM) image is shown in **Fig. S2(a)**, where the region above the red dashed line is covered with graphene. Raman spectroscopy was performed on the graphene-coated single-crystalline Au area marked by the red circle, and the resulting spectrum is presented in **Fig. S2(b)**. Two prominent peaks are observed: the G peak, corresponding to the in-plane vibrational mode of sp^2-hybridized carbon atoms, typically appears near 1587 cm^{-1}; and the 2D peak, which is the second-order overtone of the D band arising from a two-phonon scattering process, generally appears around 2675 cm^{-1} [2-3]. In our measurement, the 2D peak is located at 2681 cm^{-1}, indicating a noticeable blueshift. This shift is consistent with p-type doping of the graphene layer [3].

■ Dispersion of the effective refractive index for InP nanowires with varying diameters

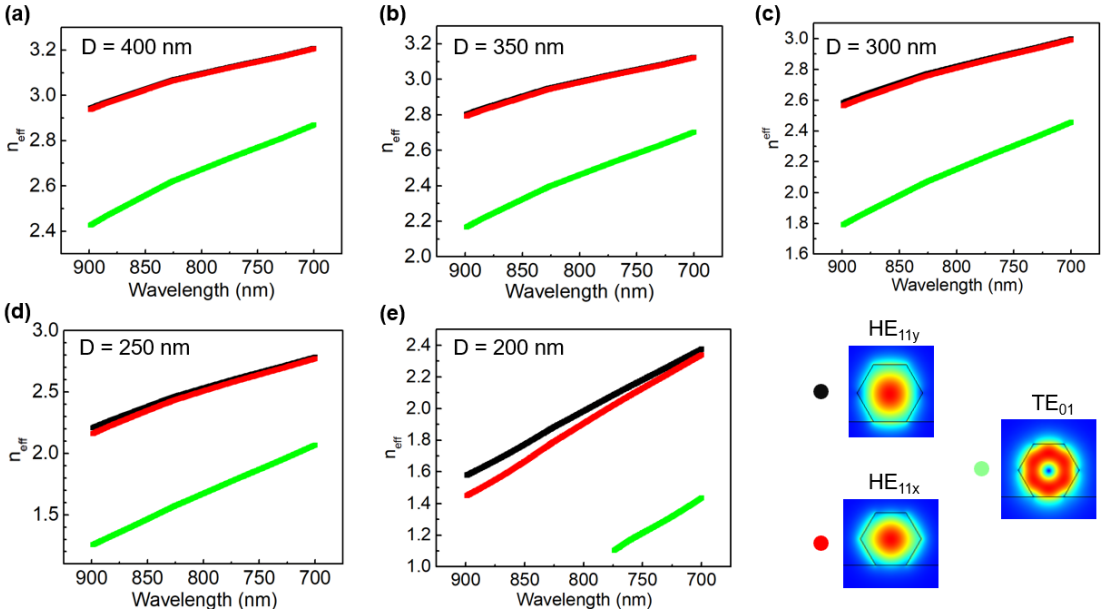

Figure S3 | Dispersion of the effective refractive index for InP nanowires on SiO_2 substrate with varying diameters (a-e) The relationship between effective refractive index and wavelength for the photonic mode is shown for InP nanowires with diameters gradually reduced from 400 nm to 200 nm in 50 nm increments. The corresponding transverse mode profiles are plotted in the bottom right.

As introduced in **Fig. 2** of the Results and Discussion section in the main text, the two HE_{11} modes exhibit a decrease in effective refractive index by reducing InP nanowire diameter due to increased mode leakage, yet they remain supported within the nanowire. In contrast, the TE_{01} mode experiences severe leakage and becomes unsustainable in nanowires when the diameter is smaller than 200 nm.

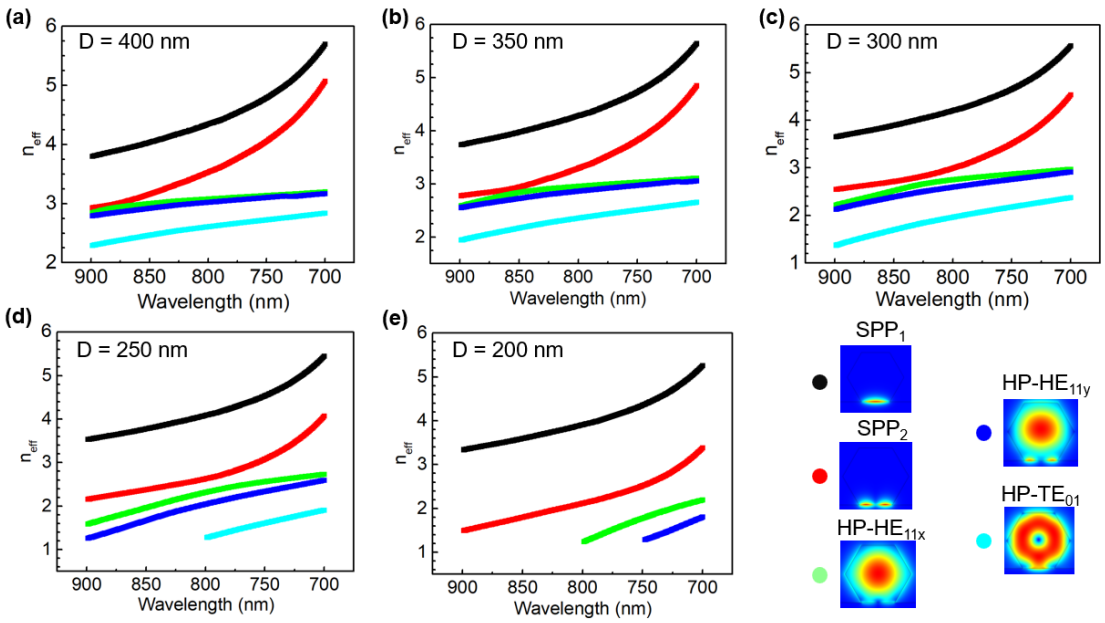

Figure S4 | Dispersion of the effective refractive index for InP nanowires on single-crystalline Au flake with varying diameters. (a-e) The relationship between effective refractive index and wavelength for the plasmonic mode is shown for InP nanowires with diameters gradually reduced from 400 nm to 200 nm in 50 nm increments. The corresponding transverse mode profiles are plotted in the bottom right.

The effective refractive indices of the two SPP modes decrease as the diameter of the InP nanowires is reduced, due to increased mode leakage; however, these modes remain supported within the nanowires. Conversely, the HP-TE_{01} mode experiences substantial leakage and ceases to be supported in nanowires when the diameter is smaller than 250 nm. Likewise, the HP-HE_{11} mode undergoes severe leakage and cannot be maintained in nanowires when the diameter is smaller than 200 nm.

■ Determination of the dominant mode in InP nanowires on SiO_2 and single-crystalline Au flake

(a)

Mode \ Diameter (nm)	400	350	300	250	200
	X	X	X	X	X
MAE (nm) 	0.5	0.51	0.73	2.34	1.54
	0.73	1	1.61	X	X
ΔMAE (nm)	0.01				
Confidence	Low (near-degenerate)				

(b)

Mode \ Diameter (nm)	400	350	300	250	200
	X	X	X	X	X
	1.29	0.66	1.28	1.57	X
MAE (nm) 	0.78	1.22	1.49	1.58	X
	X	X	X	X	X
	0.58	1.15	1.1	X	X
ΔMAE (nm)	0.2				
Confidence	Moderate				

Table S1 | MAE calculation results for dominant modes and diameters of InP nanowires (a) Calculation results of the InP nanowire on a SiO_2 substrate. The MAE separation, which is defined as $\Delta MAE = MAE_{runner\text{-}up} - MAE_{best}$ ($\Delta MAE = 0.01$ nm) is well below the experimentally observed wavelength repeatability (±0.15 nm), indicating a near-degenerate case in terms of the diameter identification. **(b)** Calculation results of the same InP nanowire on a single-crystalline Au flake. Here, $\Delta MAE = 0.20$ nm is comparable to the experimental uncertainty, providing moderate confidence when combined with polarization analysis and cavity-length consistency for the same nanowire.

For **Table. S1(a)**, corresponding to the results in **Fig. 3** of the main text, the dominant mode is determined first by analyzing the far-field polarization shown in **Fig. 3c**. Since the emission is polarized perpendicular to the nanowire axis, the HE_{11y} mode is excluded. Furthermore, as shown in **Fig. S3**, the TE_{01} mode cannot be supported when the nanowire diameter is below 250 nm, and is therefore also excluded from

consideration. Among the remaining possibilities, the calculation results indicate that a nanowire with a diameter of 400 nm dominated by the HE_{11x} mode yields the lowest mean absolute error (MAE), identifying it as the most probable configuration.

Similarly, **Table S1(b)** corresponds to the results in **Fig. 4** of the main text. The polarization analysis in **Fig. 4(d)** shows emission perpendicular to the nanowire axis, excluding the SPP_1 and HP-HE_{11y} modes. As shown in **Fig. S4**, HP-HE_{11} modes are not supported when the nanowire diameter is below 200 nm, and HP-TE_{01} modes are not supported below 250 nm, both of which are therefore omitted. Within the remaining valid parameter space, the configuration with a 400 nm nanowire dominated by the HP-TE_{01} mode yields the smallest MAE and is thus identified as the dominant lasing mode.

(a)

Mode \ Diameter (nm)	400	350	300	250	200
	X	X	X	X	X
	1.66	2.39	1.3	0.1	1.87
MAE (nm) 	2.01	1.84	2.02	2.2	X
	X	X	X	X	X
	2.41	1.89	1.19	X	X
ΔMAE (nm)	1.09				
Confidence	High				

(b)

Mode \ Diameter (nm)	400	350	300	250	200
	X	X	X	X	X
	1.74	3.06	1.81	0.25	2.12
MAE (nm) 	2.18	1.94	1.34	2.2	X
	X	X	X	X	X
	2.15	2.16	1.11	X	X
ΔMAE (nm)	0.86				
Confidence	High				

Table S2 | MAE calculation results for dominant modes and diameters of InP nanowires (a) Calculation results of the InP nanowire on a bare single-crystalline Au flake. The MAE separation (ΔMAE = 1.09 nm) is significantly larger than the experimental wavelength uncertainty, enabling high-confidence mode identification based on MAE ranking alone. **(b)** Calculation results of the same InP nanowire on a single-crystalline Au flake covered with a monolayer graphene. The large MAE

separation (ΔMAE = 0.86 nm) indicates robust mode identification. In addition, the same transverse mode family is preserved before and after graphene integration, further supporting the assignment.

For **Table S2(a)**, which corresponds to the results in **Fig. 5** of the main text, the dominant mode is identified based on the far-field polarization shown in **Fig. 5c**. Since the emission is polarized perpendicular to the nanowire axis, the SPP_1 and HP-HE_{11y} modes are excluded. In addition, **Fig. S4** indicates that HP-HE_{11} modes are not supported when the nanowire diameter is below 200 nm, and HP-TE_{01} modes are not supported below 250 nm, thereby ruling them out. Among the remaining candidates, the configuration with a 250 nm nanowire dominated by the SPP_2 mode exhibits the lowest MAE and is thus identified as the most probable dominant mode.

Similarly, **Table S2(b)** corresponds to the results in **Fig. 6** of the main text. The far-field polarization shown in **Fig. 6d** is also perpendicular to the nanowire axis, excluding the SPP_1 and HP-HE_{11y} modes. As shown in **Fig. S4**, HP-HE_{11} modes are not supported below 200 nm and HP-TE_{01} below 250 nm, which eliminates both options. Among the remaining possibilities, the simulation with a 250 nm nanowire dominated by the SPP_2 mode again yields the lowest MAE, confirming it as the most likely lasing mode.

■ Band diagram of Au and monolayer graphene

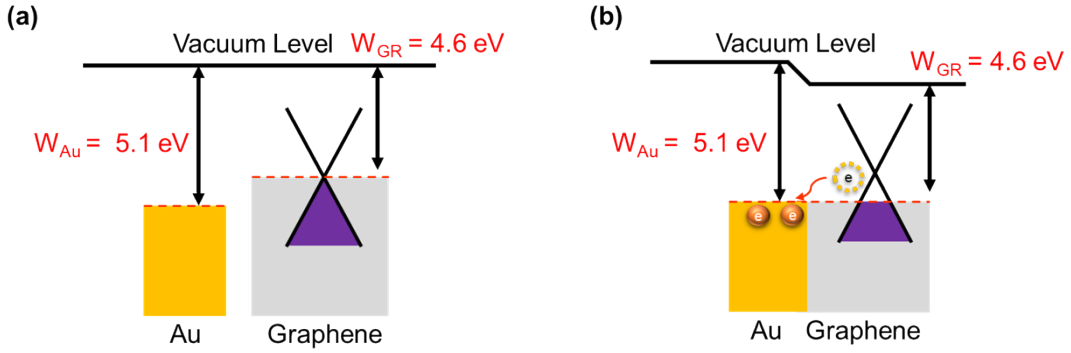

Figure S5 | Schematic illustration of the interfacial band alignment between Au and monolayer graphene Schematic energy band diagram of Au and monolayer graphene: (a) Before contact, showing the initial Fermi levels and work function difference. (b) After contact, illustrating Fermi level alignment and charge redistribution at thermal equilibrium.

Figure S5(a) illustrates the energy band alignment before contact between Au and monolayer graphene. The work function of Au is approximately 5.1 eV [4], while the work function of graphene near the Dirac point is around 4.6 eV [3], which is lower than that of Au. Upon contact, thermal equilibrium is established as shown in **Fig. S5(b)**, resulting in electron transfer from graphene to the Au surface. This charge transfer induces p-type characteristic in the graphene layer and surface charge accumulation of Au. Such band alignment and charge redistribution are consistent with the experimental observations of blueshift in both the lasing wavelength of the InP nanowire and the Raman spectra of graphene/Au.

References

1. Joyce, H.J. Wong-Leung, J. Gao, Q. Tan, H.H. Jagadish, C., "Phase Perfection in Zinc Blende and Wurtzite III−V Nanowires Using Basic Growth Parameters," *Nano Lett.,* vol. 10, no. 3(2010): 908-915.
2. Malard, L.M. Pimenta, M.A. Dresselhaus, G. and Dresselhaus, M.S., "Raman spectroscopy in graphene," *Phys. Rep.*, vol. 473(2009): 51-87.
3. Li, H. Li, J.-H. Hong, K.-B. Yu, M.-W. Chung, Y.-C. Hsu, C.-Y. Yang, J.-H. Cheng, C.-W. Huang, Z.-T. Chen, K.-P. Lin, T.-R. Gwo, S. and Lu, T.-C., "Plasmonic Nanolasers Enhanced by Hybrid Graphene–Insulator–Metal Structures," *Nano Lett.*, vol. 19, no. 8(2019): 5017-5024.
4. Rajput, R. and Vaid, R., "Flash memory devices with metal floating gate/metal nanocrystals as the charge storage layer: A status review," *FACTA UNIVERSITATIS Series Electronics and Energetics.*, vol. 33, no. 2(2020): 155-167.